Analysis using a two-layer model of the transport properties of InGaN epilayers grown on GaN template substrate

Ahmad Sauffi Yusof, Sidi Ould Saad Hamady, Christyves Chevallier, Nicolas Fressengeas, Zainuriah Hassan, Sha Shiong Ng, Mohd Anas Ahmad, Way Foong Lim, Muhd Azi Che Seliman

▶ **To cite this version:**

Ahmad Sauffi Yusof, Sidi Ould Saad Hamady, Christyves Chevallier, Nicolas Fressengeas, Zainuriah Hassan, et al.. Analysis using a two-layer model of the transport properties of InGaN epilayers grown on GaN template substrate. Materials Science in Semiconductor Processing, 2022, 144, pp.106614. 10.1016/j.mssp.2022.106614 . hal-03609434

HAL Id: hal-03609434
https://hal.science/hal-03609434v1

Submitted on 22 Jul 2024

HAL is a multi-disciplinary open access archive for the deposit and dissemination of scientific research documents, whether they are published or not. The documents may come from teaching and research institutions in France or abroad, or from public or private research centers.

L'archive ouverte pluridisciplinaire **HAL**, est destinée au dépôt et à la diffusion de documents scientifiques de niveau recherche, publiés ou non, émanant des établissements d'enseignement et de recherche français ou étrangers, des laboratoires publics ou privés.

Distributed under a Creative Commons Attribution - NonCommercial 4.0 International License

Version of Record: https://www.sciencedirect.com/science/article/pii/S1369800122001573
Manuscript_842c21d3fb392c4bb95148226ce41396

Materials Science in Semiconductor Processing 144 (2022) 106614

Contents lists available at ScienceDirect

Materials Science in Semiconductor Processing

journal homepage: www.elsevier.com/locate/mssp

Full length article

Analysis using a two-layer model of the transport properties of InGaN epilayers grown on GaN template substrate

Ahmad Sauffi Yusof [a,b,*], Sidi Ould Saad Hamady [a], Christyves Chevallier [a], Nicolas Fressengeas [a], Zainuriah Hassan [b], Sha Shiong Ng [b], Mohd Anas Ahmad [b], Way Foong Lim [b], Muhd Azi Che Seliman [b]

[a] Université de Lorraine, CentraleSupélec, LMOPS, F-57000 Metz, France
[b] Universiti Sains Malaysia, INOR, Penang, Malaysia

ARTICLE INFO

Keywords:
InGaN
Epitaxy
MOCVD
Thin-film
Characterization
Van der Pauw
Hall effect
Two-layer model
Solar cell

ABSTRACT

In this paper, a two-layer model was used to investigate the electrical properties of InGaN epilayer grown by MOCVD on a semiconducting GaN template substrate. The elaboration process was optimized to obtain high-quality InGaN epilayers with respect to the indium composition. The details of structural and optical properties as well as the surface morphology evolution were studied using X-ray diffraction, photoluminescence spectroscopy, and atomic force microscopy, respectively. The electrical transport properties were measured using the van der Pauw/Hall effect method combined with a two layer model for the first time for InGaN. The obtained experimental results combined with the developed model allowed to precisely extract the electrical properties of the InGaN epilayers and correlate them to the structural properties. The developed model procedure and code are made available and can be easily adapted to other III-N and III-V compound semiconductors grown on a semiconducting substrate.

1. Introduction

Indium gallium nitride (InGaN) ternary alloy is one of the most promising and outstanding materials for modern photonic and electronic devices. With the recent advancement of InGaN as active materials in solid-state lighting technologies, particularly in ultraviolet/blue/green light-emitting diodes to continuous wave laser diodes [1–3], a focus has been drawn into elaborating and developing the material into a high-efficiency photovoltaic application owing to its fascinating intrinsic properties [4,5]. The fundamental bandgap of InGaN alloy can be engineered from 0.67 eV (InN) to 3.4 eV (GaN), which is the only material among the III-V semiconductors (including III-Nitride) that provides an excellent spectral match with the solar spectrum. In addition, the absorption coefficient of InGaN is much higher than any other III-V material, thus making it possible to develop into thin-film solar cells. InGaN also possesses experimental carrier mobilities higher than 300 cm^2/Vs [6], high resistance to extreme conditions with an operating temperature as high as 400 °C [7,8], a high ionizing radiation tolerance with the irradiation-induced degradation in the photoluminescence intensity lower than 0.1 decade/10^{12} MeV/g [9] and a predicted lifetime better than 30 years under solar storm proton irradiation [7], and very high chemical stability [10], allowing the fabricated photovoltaic devices to be operated in a harsh environment.

The work in this area has been focused on addressing the main technological challenges, primarily on the InGaN epitaxial growth, such as the difficulty in growing high-quality In-rich monocrystalline InGaN epilayers with optoelectronic properties suitable for applications such as solar cells [11–15]. This is because almost all epitaxially grown In-rich InGaN films tend to possess phase separation and composition fluctuation within the grown structure due to the solid phase miscibility gap. The existence of the solid phase miscibility gap in InGaN alloy is related to the mismatch between the lattice parameters of the binary GaN and InN. Thus, it is essential to precisely control the InGaN epitaxial growth parameters such as growth temperature/pressure and precursor flow rate to realize high-quality In-rich InGaN films. Indeed, the impurities and other strain-related defects such as point, and V-defect can be introduced into the epitaxial films during the growth process due to the mismatch. These defects can contribute as a recombination site for the photoexcited carriers, lowering the overall photovoltaic properties of the fabricated devices, such as lower short circuit current density and shorter carrier lifetime. Nonetheless, the created defects induced by the mismatch can be partially mitigated by using the GaN template. This method has been demonstrated in LED technology, where thin InGaN multi-quantum wells with low indium

* Corresponding author at: Université de Lorraine, CentraleSupélec, LMOPS, F-57000 Metz, France.
E-mail address: ahmad-sauffi.yusof@univ-lorraine.fr (A.S. Yusof).

https://doi.org/10.1016/j.mssp.2022.106614
Received 20 December 2021; Received in revised form 11 February 2022; Accepted 25 February 2022
Available online 11 March 2022
1369-8001/© 2022 Elsevier Ltd. All rights reserved.

© 2022 published by Elsevier. This manuscript is made available under the CC BY NC user license
https://creativecommons.org/licenses/by-nc/4.0/

composition can be grown relatively in strain when heteroepitaxially grown on a thick GaN buffer layer [16]. However, through this transverse structure configuration, it is known that the outcome of the crystal quality, as well as the electrical and optical properties of the InGaN epilayer are heavily dependent on the buffer layer/substrate condition.

For instance, the electronic properties of an active layer grown on a semiconducting substrate are particularly challenging to investigate using a typical electrical characterization method such as the Hall effect with van der Pauw configuration since the underlying thick semiconducting GaN template can strongly influence the outcome of the measured electrical transport properties such as resistivity, carrier concentration, and mobility. The necessity to grow InGaN on a semiconducting substrate in our case is justified by two reasons. First, the final objective of optimizing InGaN/GaN is the development of InGaN-based solar cells in the transverse configuration where the bottom layer should be highly doped for the deposition of ohmic contact. Second, the optoelectronic properties of III-Nitride materials depend on the substrate and a study on a particular substrate cannot be extrapolated to a different one. To overcome this limitation, we proposed for the first time for InGaN/GaN heterostructures a two-layer methodology using the theoretical formalism in [17] to investigate the transport properties of the InGaN epilayer grown in such structure configuration. This model extends the classical two-layer approach developed for layers with different types and/or for non-isolated layers either with top or lateral contacts [18,19]. This classical procedure is inherently not adapted to InGaN/GaN heterostructure where the conduction between the InGaN epilayer and the semiconducting GaN substrate under the contact region as well as the conduction in the substrate itself dominates the measured electrical characteristics. The main advantage of the method used in this work is the fact that it takes into account the contribution of the GaN substrate and the conduction between it and the InGaN epilayers, permitting to achieve reliable and high precision van der Pauw and Hall effect measurements for the same InGaN/GaN heterostructure that will be used in the actual device. The procedure was applied to perform a study of the transport properties of InGaN epilayer with respect to indium composition ranging from about 4% up to 11%. Using this approach, the transport properties of the InGaN epilayers are discussed in conjunction with a detailed study of the structural properties using X-ray diffraction, atomic force microscopy, and photoluminescence spectroscopy. The developed code of the two-layer model analysis for the van der Pauw and Hall effect characterization method is made available and can be easily adapted to other materials where the active layer is grown on a semiconducting substrate.

The study of the transport properties, using this two-layer method, of InGaN/GaN heterostructure elaborated using MOCVD and characterized using X-ray diffraction, photoluminescence and AFM technique, is presented with, first, the experimental procedure described in Section 2. Then, Section 3 presents the structural and morphological properties of the elaborated layers. Section 4 develops in detail the two-layer method and its application to InGaN/GaN and discusses the correlation between the extracted electrical properties and the structural properties.

2. Elaboration and characterization procedure

The InGaN/GaN heterostructures were epitaxially grown using the Taiyo Nippon Sanso Corporation (TNSC) MOCVD SR4000-HT system on 3.850 μm thick GaN/sapphire substrate. During the epitaxial process, triethylgallium (TEGa), trimethylindium (TMIn) and NH_3 were used as gallium, indium and nitrogen precursors respectively with N_2 as the carrier gas for InGaN layers. The indium composition in the grown InGaN epilayer can be varied by changing either the metal–organic source flows or the growth temperature. In the MOCVD horizontal reactor system we used, the indium composition within the grown structure is predominantly determined by the growth temperature operation while not significantly affected by the TMIn flow rate, as already reported in literature [20,21]. When using the first method, varying the metal–organic source flows, we observed the formation of indium droplets on epitaxially grown InGaN films, due to the reduction in the V/III ratio. This can result in the subsequent deficit of nitrogen precursor leading to In-N bond dissociation, and subsequently reduced the quality of the grown structure. In contrast, by varying the growth temperature and keeping the same optimized metal–organic source flows, we did suppress the formation of indium droplets as well as maintaining the crystal quality of the grown structure characterized by mean of XRD, AFM and PL. Thus, we varied the growth temperature settings between 860 °C and 820 °C in order to manipulate the indium composition within the grown structure, while keeping constant the other growth parameters (flow rates, V/III and TMI/III ratios, growth duration, cf. Table 1). The repeatability of the MOCVD elaboration process was verified by repeating the InGaN growth several times with the same combination of the elaboration parameters. In addition, the InGaN layers were elaborated on different GaN/Sapphire substrates, with similar doping which is necessary to our application, to further optimize the growth process and to check the proposed two-layer model robustness.

The crystallinity and defect density of the grown InGaN/GaN heterostructures were investigated using the high-resolution X-ray diffraction (HR-XRD, Bruker D8 Discover) system with a triple-axis configuration on symmetric (0002). The indium composition of the epitaxial layer was estimated through the analysis of the XRD triple-axis curves.

A field emission scanning electron microscope (FE-SEM, FEI Nova NanoSEM 450) and atomic force microscopy (AFM, Dimension EDGE Bruker) was used to observe the surface morphology, structural changes, and thickness of the grown structure. The optical properties of the grown structures were investigated by using photoluminescence spectroscopy (LabRam HR 800 UV, Horiba Jobin-Yvon).

The electrical transport properties of the grown InGaN/GaN heterostructures were measured using the van der Pauw/Hall effect technique in all configurations and with respect to the current intensity using a home-made setup with a 0.55 T permanent magnet and two source-measure units (SMU) from Keithley (2602 and 2636B models). The acquisition and analysis procedures are fully automated using software developed internally. The implementation of the two-layer model to extract the electrical transport properties of the grown InGaN epilayer is detailed in Section 4.

3. Morphology and structural properties

To study the growth of InGaN/GaN and to prepare the grown samples for the electrical measurements, we conducted a comprehensive analysis of the morphology and structural properties using XRD, PL and AFM in the conditions detailed in the previous Section 2.

Fig. 1(a) shows the $\omega - 2\theta$ scan on symmetry (0002) of InGaN/GaN heterostructure as a function of InGaN growth temperature (860 °C, 840 °C and 820 °C). The main difficulty associated with elaborating InGaN thin films is related to the high saturation of InN vapor pressure [22,23] that can be partially addressed by lowering the growth temperature to enhance the indium incorporation. However, at relatively low temperatures, ammonia dissociation will become inefficient. It is thus necessary to optimize rigorously the temperature range to elaborate single phase monocrystalline InGaN layers. In our case, the optimized range corresponds to a growth temperature between 820 °C and 860 °C. In this range, the indium compositions were estimated through the analysis of the diffractograms with values 4.02%. 6.56%, and 10.86% for the InGaN epilayers grown at 860 °C, 840 °C, and 820 °C, respectively. The extracted lattice parameter shows an increasing linear trend as a function of indium composition as shown in Fig. 1(b), suggesting that different amounts of indium have been successfully integrated into the structure. It should also be noted that

Table 1
InGaN/GaN samples main MOCVD elaboration parameters. The layers thicknesses were measured using field emission scanning electron microscopy. The InGaN thickness is about 350 nm for all considered compositions. The TEG and TMI flow rates were fixed at 69.3 sccm and 184 sccm respectively; the V/III and TMI/III ratios were fixed at 15777 and 57% respectively.

Structure	Growth temperature (°C) and duration	Indium composition x (%) from XRD	Indium composition x (%) from PL	Total thickness (μm)
GaN/sapphire	1120 60 minutes	–	–	3.850
InGaN/GaN/sapphire	860 direct growth 252 minutes	04.02	03.91	4.200
InGaN/GaN/sapphire	840 direct growth 252 minutes	06.46	06.64	4.200
InGaN/GaN/sapphire	820 direct growth 252 minutes	10.86	11.50	4.200

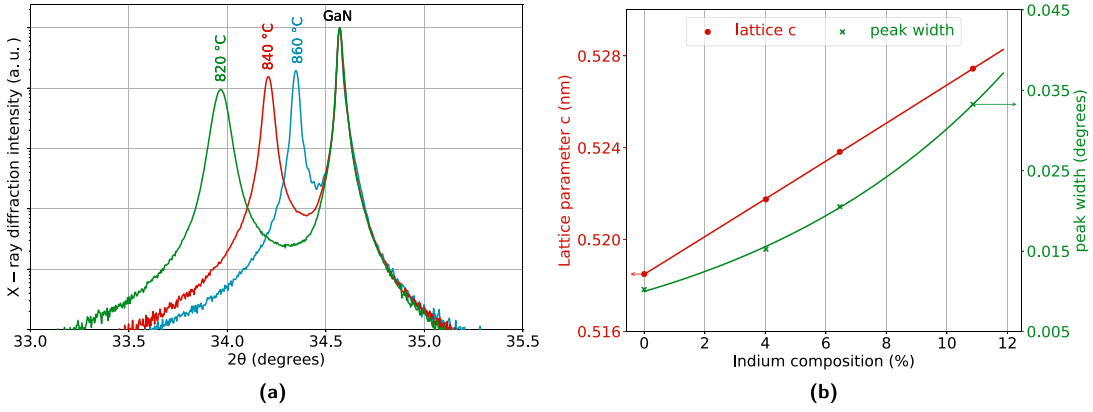

Fig. 1. 1(a) & 1(b): XRD diffractograms of InGaN/GaN heterostructures and the InGaN lattice parameter and peak width with respect to the InGaN growth temperature. The extracted indium compositions are: 04.02% for a growth temperature of $T = 860$ °C; 06.46% for $T = 840$ °C and 10.86% for $T = 820$ °C.

no additional peaks related to InN/GaN phases were detected within the sensitivity of the instrument, indicating that the epilayers were successfully grown without any existence of phase separation. However, decline in the peak intensity, as well as the broadening of the peak width, seen in as a function of InGaN growth temperature, which suggests that there is an overall decline in the quality of the grown structure as usually observed in the III-N alloys [24,25].

In order to additionally verify the indium composition and the structural properties derived from the XRD results analysis, photoluminescence (PL) spectroscopy measurements were carried out by exciting the grown InGaN/GaN heterostructure using 325 nm of He–Cd laser with fixed excitation power at 20 mW. The PL spectra of the three samples are shown in Fig. 2. The plot shows that all structures possess a distinct band edge emission peak at 382.7 nm, 396.2 nm, and 421.8 nm, corresponding to the InGaN epilayer grown at 860 °C, 840 °C, and 820 °C, respectively with a weak broad emission band most likely originating from nitrogen vacancies [26]. These deep levels are probably formed due to the reduction in the ammonia dissociation, which is related to the InGaN growth temperature. The redshift in the band edge emission peak is also observed when the growth temperature of the InGaN layer is reduced, indicating the enhancement of the indium incorporation in the grown InGaN epilayer. The indium composition estimated through PL spectroscopy was at 3.91%. 6.64% and 11.5% for the InGaN epilayer grown 860 °C, 840 °C, and 820 °C, respectively. The obtained values of the indium composition through this method are in good agreement with the value obtained through the analysis of the XRD curve. The PL spectra, with no additional InN/GaN phases related peaks, also indicate that the InGaN layer was successfully grown without any occurrence of phase separation, which are similarly shown in the XRD measurements.

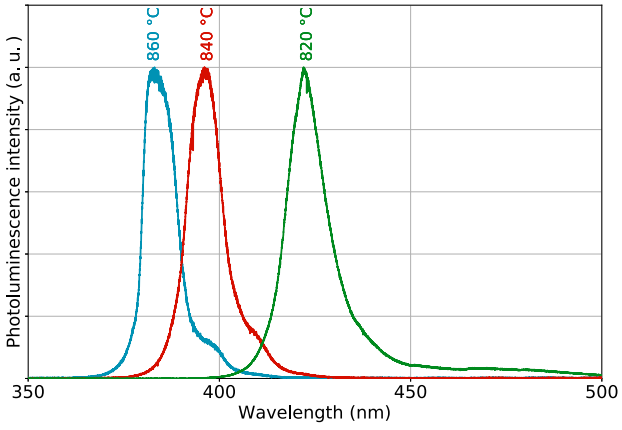

Fig. 2. Room temperature normalized photoluminescence spectra of InGaN/GaN heterostructure as a function of InGaN growth temperature. The extracted indium compositions are 03.91% for a growth temperature of $T = 860$ °C; 06.64% for $T = 840$ °C and 11.50% for $T = 820$ °C.

To complete the structural study, we investigate the evolution of the surface morphology of the grown InGaN/GaN heterostructure as a function of indium composition: an AFM measurement with a 5×5 μm scan area was carried out on the surface of the grown InGaN/GaN heterostructure as shown in Fig. 3(a), 3(b), and 3(c). From observation, no indium droplets were detected on the surface of the grown structure within the AFM scan area. The AFM topography image reveals that all structure depicts a clear step and terrace feature, which indicates

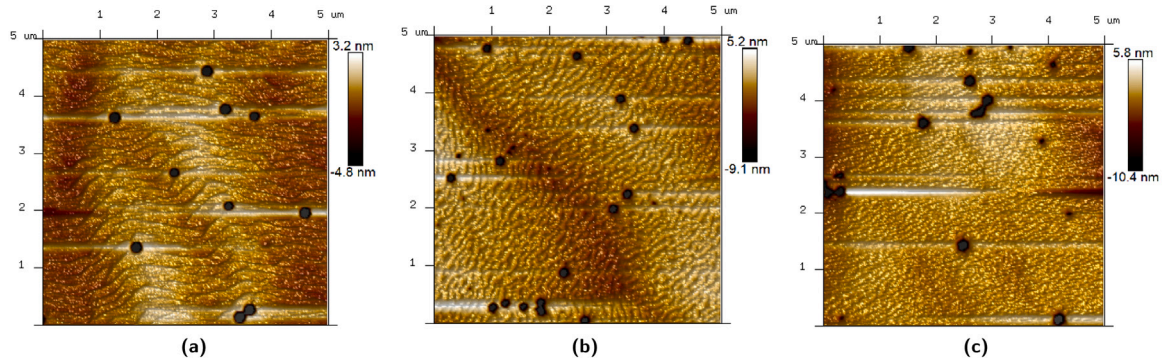

Fig. 3. AFM images of InGaN/GaN heterostructure with different indium compositions: 04.02% (3(a)); 06.46% (3(b)) & 10.86% (3(c)).

that the InGaN epilayer's growth process was dominated by step-flow growth mode [27,28]. Although the surface show dense and continuous morphology, multiple formations of V-pits can be seen on the surface of the grown structure. The V-pits' formation can be attributed to the interaction between the step structure and dislocations introduced by the strain during the growth process. The introduced screw and other mixed type dislocation originated from the mismatch, and alloy disordering will seize the advancement of the surface terrace step and cause it to bow out from the initial point, resulting in the formation of the observable V-pits [29]. Moreover, the increase in the indium composition also can induce an additional internal strain within the grown structure, which can be released through threading dislocation and stacking faults. As a result, it will reduce the quality of the grown structure. This effect is similarly observed in the reduction of the XRD intensity peak as shown in Fig. 1(b) and the increase the density and size of the V-pits for InGaN epilayer with high indium composition. The RMS surface roughness was slightly increased from 1.2 nm to 1.8 nm for structures with 4% and 11% indium composition, respectively. This behavior can be attributed to the Ehrlich–Schwoebel barrier (ESB), which involves the kinetic barrier energy at the growth surface step-edge [30].

4. Electrical characterization and two-layer model

After the optimization of the growth conditions and the analysis of the morphology and structural properties of the InGaN epilayers on GaN, a detailed electrical study was conducted in order to understand the impact of the growth conditions on the electrical properties. As detailed in the introduction, the main challenge when electrically characterizing the InGaN/GaN heterostructure is the contribution of the GaN layer to the conduction. In the following sections, the two-layer model and its application to this structure is detailed. First, the electrical characterization protocol is presented and, second, the two-layer model is developed and, last, the application of the model to the InGaN epilayers on GaN is investigated and the results correlated to the structural properties discussed in the previous sections.

4.1. Experimental protocol

The electrical measurements were done using the van der Pauw/Hall effect technique in all configurations and with respect to the current intensity using the setup described in the experimental procedure Section 2. For all samples, indium was deposited to form the four ohmic contacts and the ohmicity was systematically checked and the contacts size was kept sufficiently small compared to the distance between them. Figs. 4(a) and 4(b) show configurations used for the van der Pauw and Hall measurements. To accurately measure the transport parameters using this technique, it is mandatory to acquire a large set of data by changing the geometry and by varying the current and the magnetic field direction. In particular, the Hall voltage is impacted by a large offset due to the geometry (sample shape, contact size and placement, etc.) and the current-induced heating. Using such a rigorous procedure permits to extract precisely the parameters from the data set. Reference samples of zinc oxide (ZnO), indium tin oxide (ITO) and ZnO/ITO on sodalime glass were used in order to check the accuracy and robustness of the electrical characterization procedure and the two-layer model.

From the measurements in the van der Pauw configuration, the resistivity ρ is obtained by exactly solving the classic van der Pauw equation (1) knowing the film thickness and measuring R_1 and R_2:

$$exp\left(-\pi\frac{R_1}{\rho/t}\right)+exp\left(-\pi\frac{R_2}{\rho/t}\right) = 1 \quad (1)$$

The R_1 and R_2 resistances are extracted by measuring the voltages in different geometries and by reversing the current for each geometry:

- $(V_{AB},\ I_{DC})$; $(V_{BA},\ -I_{DC})$; $(V_{DC},\ I_{AB})$; $(V_{CD},\ -I_{AB})$
- $(V_{BC},\ I_{DA})$; $(V_{CB},\ -I_{DA})$; $(V_{DA},\ I_{BC})$; $(V_{AD},\ -I_{BC})$

$(V_{AB},\ I_{DC})$ means that the current is injected between D and C (cf. Fig. 4(a)) and voltage measured between A and B, and equivalently for the following notations. The resistivity ρ is acquired with respect to the injected current, varying in a relatively large current range, to ensure the accuracy and robustness of the measurements.

For the Hall configuration, the Hall voltage V_H is extracted from the set of measurements by varying the current, reversing the magnetic field and changing the geometry:

- $(V_{AC},\ I_{DB},\ +B)$; $(V_{AC}, I_{DB},\ -B)$; $(V_{CA},\ -I_{DB},\ +B)$; $(V_{CA},\ -I_{DB},\ -B)$
- $(V_{DB},\ I_{AC},\ +B)$; $(V_{DB},\ I_{AC},\ -B)$; $(V_{BD},\ -I_{AC},\ +B)$; $(V_{BD},\ -I_{AC},\ -B)$

$(V_{AC},\ I_{DB},\ +B)$ means that the current is injected between D and B, the magnetic field B applied in the direction taken as positive and the voltage measured between A and C (cf. Fig. 4(b)). Then the extracted Hall voltage V_H for a given current I and magnetic field B is used to calculate the carrier concentration n:

$$V_H = \frac{I\ B}{n\ q\ t} \quad (2)$$

Where q is the elementary charge and t the sample thickness. The carrier mobility is deduced from n and ρ.

The measurements include of course the whole heterostructure and therefore the contribution of the epilayer and that of the substrate cannot be discriminated, particularly when the substrate is thick and conductive. This is why using the two-layer model presented in the next section is crucial to extract the epilayer transport properties.

4.2. Two-layer model

Considering the InGaN/GaN heterostructure, schematically represented in Figs. 4(a) and 4(b) in the van der Pauw/Hall configuration with top placed contacts, the whole structure conductivity σ and

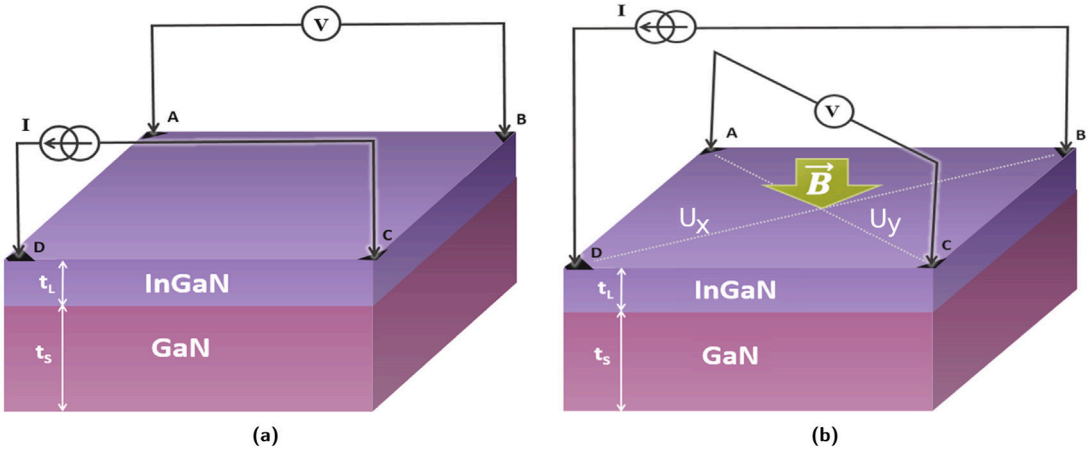

Fig. 4. Van der Pauw (4(a)) & Hall (4(b)) configurations for the measurement of resistivity and carrier concentration of InGaN/GaN thin films. In Fig. 4(b), U_x is the applied voltage in a given x direction corresponding to the injected current and U_y is the open-circuit induced Hall voltage.

mobility μ are given by the following equations [17]:

$$\begin{aligned}\sigma &= \frac{U_{x,L}\,t_L}{U_x\,t}\sigma_L + \frac{U_{x,S}\,t_S}{U_x\,t}\sigma_S \\ \mu &= \frac{U_{x,L}U_{y,L}\,\sigma_L\,t_L}{U_xU_y\,\sigma\,t}\mu_L + \frac{U_{x,S}U_{y,S}\,\sigma_S\,t_S}{U_xU_y\,\sigma\,t}\mu_S\end{aligned} \tag{3}$$

Where index L refers to the InGaN epilayer and S to the GaN substrate; $U_{x,L}$ is the applied voltage (in a given x direction corresponding to the injected current) to the epilayer and $U_{x,S}$ the applied voltage to the substrate; $U_{y,L}$ is the voltage induced in the epilayer by the Hall effect (in the direction y of the measured Hall voltage, perpendicular to x) and $U_{y,S}$ the induced voltage in the substrate; U_x is the total applied voltage; t_L is the epilayer thickness and t_S the substrate thickness; t is the total structure thickness. σ_L and σ_S are the conduction of the epilayer and the substrate, respectively. Relations (3) are simply derived from the fact that: (i) the total current in the direction corresponding to the applied voltage is the sum of partial currents in the epilayer and substrate; (ii) the mobility is given by the relation between the injected current, related to the applied voltage (in the x direction), and the open-circuit measured Hall voltage (in the y direction) under the applied magnetic field (cf. Fig. 4(b)). In this two-layer structure, one can model the voltage $U_{x,L}$ (and $U_{x,S}$) and the corresponding current with a resistance $R_{x,L}$ for the epilayer and $R_{x,S}$ for the substrate. In the same way, the Hall induced voltage is represented by resistances $R_{y,L}$ and $R_{y,S}$. Using such an equivalent circuit formalism, one can write the voltages as following:

$$\begin{aligned}U_{x,L} &= U_x\frac{R_{x,L}}{R_{x,L}+r_{x,L}} \\ U_{y,L} &= U_y\frac{R_{y,L}}{R_{y,L}+r_{y,L}} \\ U_{x,S} &= U_x\frac{R_{x,S}}{R_{x,S}+r_{x,S}} \\ U_{y,S} &= U_y\frac{R_{y,S}}{R_{y,S}+r_{y,S}}\end{aligned} \tag{4}$$

Where $r_{x,L}$ and $r_{x,S}$ correspond to the series resistance, in the region under the contacts, between the contact and the epilayer, and the epilayer with the substrate, respectively. Similarly $r_{y,L}$ and $r_{y,S}$ are the series resistances for the y direction.

Simplifying Eq. (3) using relations in (4) gives the expression of the conductivity σ and mobility μ of the whole InGaN/GaN heterostructure as follows:

$$\begin{aligned}\sigma &= \eta_{x,L}\frac{t_L}{t}\sigma_L + \eta_{x,S}\frac{t_S}{t}\sigma_S \\ \mu &= \eta_{x,L}\eta_{y,L}\frac{\sigma_L\,t_L}{\sigma\,t}\mu_L + \eta_{x,S}\eta_{y,S}\frac{\sigma_S\,t_S}{\sigma\,t}\mu_S \\ \eta_{x,L} &= \frac{R_{x,L}}{R_{x,L}+r_{x,L}} \\ \eta_{y,L} &= \frac{R_{y,L}}{R_{y,L}+r_{y,L}} \\ \eta_{x,S} &= \frac{R_{x,S}}{R_{x,S}+r_{x,S}} \\ \eta_{y,S} &= \frac{R_{y,S}}{R_{y,S}+r_{y,S}}\end{aligned} \tag{5}$$

Where the parameters η are defined as correction factors depending on the resistances of the epilayer and the substrate and the series resistances between the layers. The determination of these parameters η in our case is crucial since it permit to reliably extract the epilayer conductivity and mobility knowing the substrate ones by taking into account the series resistance between the epilayer and the substrate in the region under the contacts. If equal to the unity, the equations give the classical case of negligible series resistance between the layers.

In the squared configuration we used (Figs. 4(a) and 4(b)), $\eta_{x,L}$ and $\eta_{y,L}$ can be considered equal: $\eta_{x,L} = \eta_{y,L} = \eta_L$ and $\eta_{x,S} = \eta_{y,S} = \eta_S$. We made a second assumption by considering negligible the series resistance between the top placed contacts and the epilayer. This assumption is well justified considering the four-probe configuration and the very low contact resistance of the soldered indium contacts. Thus the only series resistance is the one between the epilayer and the substrate. Then with $\eta_L \approx 1$ and $\eta_S = \eta$ we can rewrite Eq. (5) as:

$$\begin{aligned}\sigma &= \frac{t_L}{t}\sigma_L + \eta\frac{t_S}{t}\sigma_S \\ \mu &= \frac{\sigma_L\,t_L}{\sigma\,t}\mu_L + \eta^2\frac{\sigma_S\,t_S}{\sigma\,t}\mu_S\end{aligned} \tag{6}$$

With this two equations, the objective is to extract the epilayer conductivity σ_L and mobility μ_L by knowing the substrate conductivity σ_S and mobility μ_S as well as the whole heterostructure conductivity σ and mobility μ, with a given correction factor η:

$$\begin{aligned}\sigma_L &= \frac{t}{t_L}\sigma - \eta\frac{t_S}{t_L}\sigma_S \\ \mu_L &= \frac{\sigma\,t}{\sigma_L\,t_L}\mu - \eta^2\frac{\sigma_S\,t_S}{\sigma_L\,t_L}\mu_S \\ &= \frac{\sigma\,t\,\mu - \eta^2\,\sigma_S\,t_S\,\mu_S}{\sigma\,t - \eta\,\sigma_S\,t_S}\end{aligned} \tag{7}$$

The fact that μ_L as a function of η exhibits a maximum value in our case, therefore, η can be utilized to calculate σ_L and μ_L by using Eq. (7).

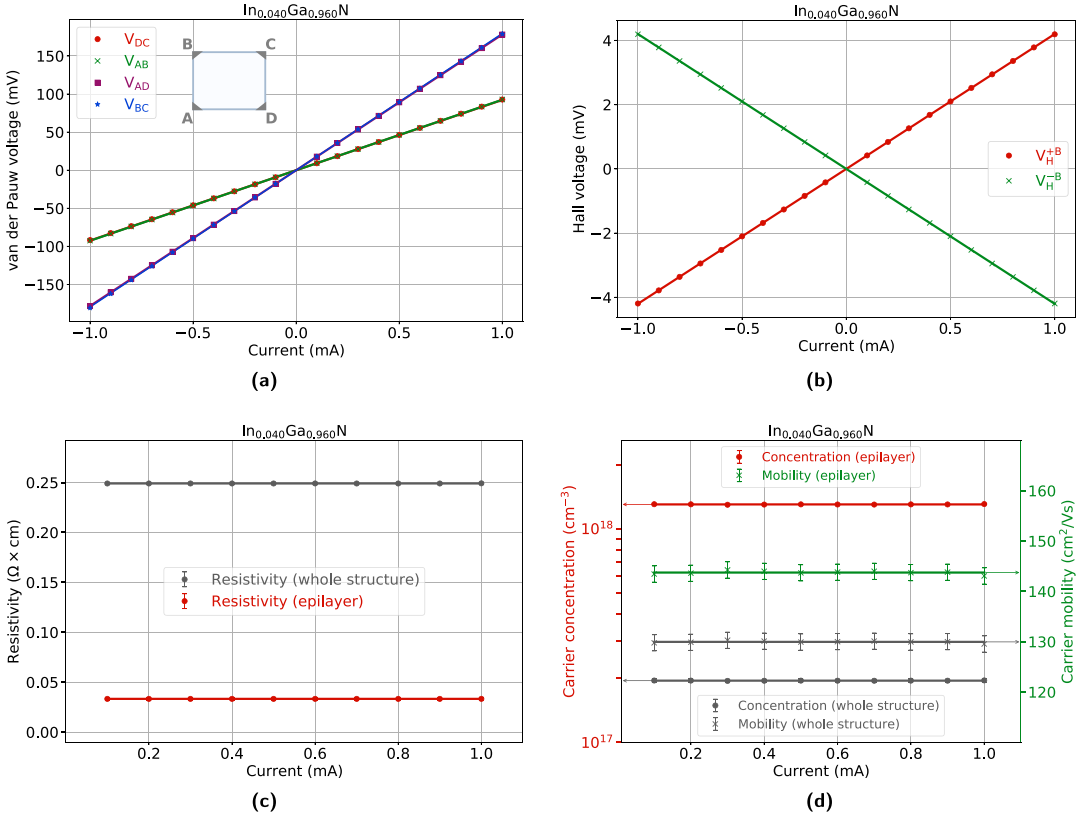

Fig. 5. 5(a): Van der Pauw voltages with respect to the injected current with the nomenclature defined in 4.1; 5(b): Hall voltages, corrected from the voltage offset, with respect to the injected current and for the two forward and reverse magnetic field; 5(c) & 5(d): Resistivity, carrier concentration and mobility for InGaN/GaN structure with an indium composition of 04.02%. For the resistivity and carrier concentration, the error bars are plotted even if they are not clearly visible due to the log scale (for concentration) and their small values (for resistivity).

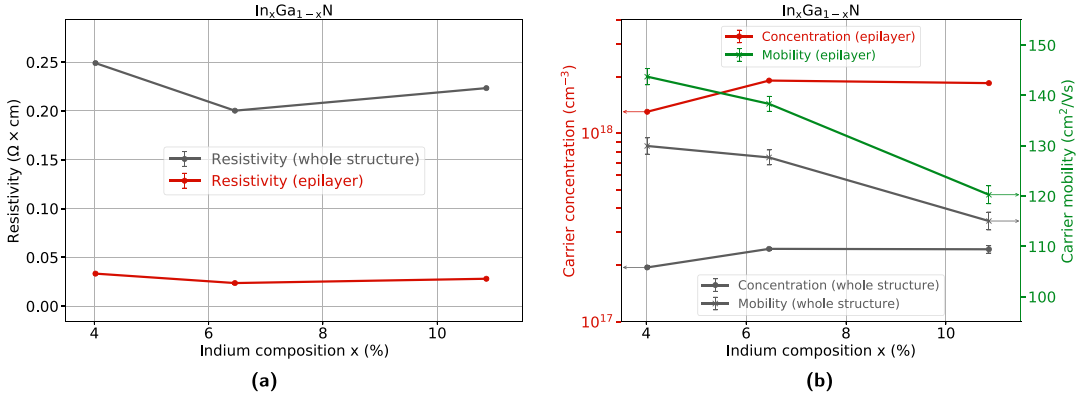

Fig. 6. 6(a) & 6(b): Resistivity, carrier concentration and mobility for InGaN/GaN structure and the extracted InGaN epilayer values, with respect to the indium composition.

4.3. Application to InGaN/GaN

We applied the two-layer model to the InGaN/GaN heterostructure with a varying indium composition. The GaN substrate transport parameters σ_S and μ_S were independently measured, using the procedure described in 4.1 and the obtained values are given in Table 2.

Figs. 5(a), 5(b), 5(c) and 5(d) show the van der Pauw and Hall voltages characteristics as well as the resistivity, carrier concentration and mobility for InGaN/GaN heterostructure with an indium composition of 04.02% in the conditions detailed in Section 4.1. The elaboration parameters of InGaN/GaN are given in Table 1. The resistivity remains almost constant with the injected current with no indication of layer heating that could induce a change in its value. The extracted Hall voltage, corrected from the voltage offset, displays an excellent linearity with the injected current permitting a reliable and precise carrier concentration determination. For this sample with 04.02% of indium, the epilayer carrier concentration (1.3×10^{18} cm^{-3}) is much higher than the concentration in the GaN substrate (9.8×10^{16} cm^{-3}, given in Table 2) and that of the whole InGaN/GaN structure (1.94×10^{17} cm^{-3}). The relatively

Table 2
The GaN/sapphire substrate mobility, conductivity and carrier concentration. The GaN thickness was measured using field emission scanning electron microscopy as for InGaN/GaN heterostructures.

Thickness t_S (μm)	Conductivity σ_S (Ω^{-1}cm^{-1})	Mobility μ_S (cm^{2}V^{-1}s^{-1})	Concentration n_S (cm^{-3})
3.850 ± 0.010	2.734 ± 0.005	174 ± 1	$(9.8\pm0.2)\times10^{16}$

high unintentional background doping in GaN grown by MOCVD is a well-known phenomenon tentatively attributed, among other origins, to nitrogen vacancy V_N or to substitutional oxygen O_N [31,32]. The increase of the carrier concentration for InGaN when compared to GaN is observed in our epilayers as shown in Fig. 5(d) for 04.02% of indium. Lozac'h et al. [33] studied the deep defects in InGaN using DLTS (Deep Level Transient Spectroscopy) and admittance spectroscopy, and identified a shallow donor state that could be related to indium fluctuation. Indeed, the formation energy of nitrogen vacancy V_N (supposed to explain, at least partially, the unintentional doping in GaN) decreased with the increase of the number of adjacent indium sites that can form a single donor [34]. Thus, the increase of the indium composition induces an increase in the unintentional background doping that can be attributed to this indium fluctuation.

Figs. 6(a) and 6(b) shows resistivity, carrier concentration, and mobility of the grown InGaN/GaN heterostructure with the indium composition ranging from about 4% to 11%. The carrier concentration slightly increases with indium composition. For a composition of 10.86% the carrier concentration is almost at the same value than that for the lower composition. This behavior could indicate an incorporation of acceptor-like defects, such as carbon, acting as trapping sites for electrons and partially compensate the increasing donor concentration induced by indium. In addition to the point defects mentioned above, dislocations, in general, play a crucial role in defining the transport properties of the grown structure, such as mobility, resistivity, and carrier concentration. The defect centers introduced during the growth process can substantially influence the carrier transition. It is expected that by increasing the indium content in InGaN alloy, the mobility will increase due to lower electron effective mass since the effective mass parameter of GaN and InN are $0.2m_0$ and $0.11m_0$, respectively, with m_0 is the free electron mass. In this work, however, the reduction in mobility can be clearly observed as the indium composition increased, similarly, reported in previous literature [35]. This trend can be associated with the enhancement in the alloy disordering effect, which can be evidently shown in the XRD and AFM results where the broad and low-intensity peak of the XRD curve (Fig. 1(b) and Section 3) as well as the increase in the surface roughness can be observed as a function of increasing indium composition. This indicates that the structure experiences a degradation in the crystal quality caused by the extended defects such as screw and other mixed type dislocation that can induce high dislocation scattering of electrons.

5. Conclusions

In this work, a two-layer model was developed to study the electrical properties of InGaN epilayers grown by MOCVD on GaN template substrate. The growth conditions were optimized to obtain InGaN monocrystalline single phase for indium composition up to 11% and the structural properties were investigated using complementary characterization techniques. The growth on a semiconducting GaN template substrate, which was required for the application, necessitated the development of the proposed method to obtain the InGaN epilayer transport properties from van der Pauw and Hall effect measurements on the InGaN/GaN heterostructure. The obtained results correlate well with the structural properties and give a reliable way to electrically characterize III-N heterostructures with the active layer elaborated on a semiconducting substrate. The developed method for InGaN can be easily extended to other III-Nitride and III-V materials. All the experimental data and the developed code are open and made available.

CRediT authorship contribution statement

Ahmad Sauffi Yusof: Writing – original draft, Methodology, Data curation. **Sidi Ould Saad Hamady:** Formal analysis, Software, Writing – review & editing. **Christyves Chevallier:** Writing – review & editing, Validation. **Nicolas Fressengeas:** Conceptualization, Formal analysis. **Zainuriah Hassan:** Supervision, Methodology. **Sha Shiong Ng:** Conceptualization. **Mohd Anas Ahmad:** Resources. **Way Foong Lim:** Visualization. **Muhd Azi Che Seliman:** Investigation.

Declaration of competing interest

The authors declare that they have no known competing financial interests or personal relationships that could have appeared to influence the work reported in this paper.

Acknowledgments

This research was supported by "Partenariats Hubert Curien (PHC) Hibiscus" in the framework of the "Hector" research project. The authors gratefully acknowledge Queny Kieffer from the Carel Platform of the LMOPS laboratory for his help in conducting the electrical measurements. Support from Universiti Sains Malaysia Fellowship is also gratefully acknowledged.

References

[1] T. Mukai, M. Yamada, S. Nakamura, Characteristics of InGaN-based UV/blue/green/amber/red light-emitting diodes, Japan. J. Appl. Phys. 38 (1999) 3976–3981.
[2] S. Nakamura, Current status and future prospects of InGaN-based laser diodes, JSAP Internat. 1 (2000) 5–17.
[3] A. Avramescu, T. Lermer, J. Müller, S. Tautz, D. Queren, S. Lutgen, U. Strauß, InGaN Laser diodes with 50 mW output power emitting at 515 nm, Appl. Phys. Lett. 95 (4) (2009) 071103.
[4] J. Wu, W. Walukiewicz, W. Shan, K.M. Yu, III.J.W. Ager, S.X. Li, E.E. Haller, H. Lu, W.J. Schaff, Temperature dependence of the fundamental band gap of InN, J. Appl. Phys. 95 (2003) 4457–4460a.
[5] W. Sun, C.K. Tan, N. Tansu, III-Nitride Digital alloy: Electronics and optoelectronics properties of the InN/GaN ultra-short period superlattice nanostructures, Sci. Rep. 7 (1) (2017) 6671.
[6] S. Surender, S. Pradeep, K. Prabakaran, S.M. Sumithra, S. Singh, K. Baskar, The role of indium composition on thermo-electric properties of InGaN/GaN heterostructures grown by MOCVD, J. Alloys Compd. 734 (2018) 48–54.
[7] D.H. Lien, Y.H. Hsiao, S.G. Yang, M.L. Tsai, T.C. Wei, S.C. Lee, J.H. He, Harsh photovoltaics using InGaN/GaN multiple quantum well schemes, Nano Energy 11 (2015) 104–109.
[8] Y. Zhao, X. Huang, H. Fu, H. Chen, Z. Lu, J. Montes, I. Baranowski, InGaN-Based solar cells for space applications, in: 2017 IEEE 60th International Midwest Symposium on Circuits and Systems (MWSCAS), IEEE, 2017, pp. 954–957.
[9] J. Wu, W. Walukiewicz, K.M. Yu, W. Shan, III.J.W. Ager, E.E. Haller, H. Lu, W.J. Schaff, W.K. Metzger, S. Kurtz, Superior radiation resistance of In(1-x)Ga(x)N alloys: Full-solar-spectrum photovoltaic material system, J. Appl. Phys. 94 (10) (2003) 6477–6482b.
[10] S.A. Kazazis, E. Papadomanolaki, E. Iliopoulos, Tuning carrier localization in In-rich InGaN alloys: Correlations between growth kinetics and optical properties, J. Appl. Phys. 127 (22) (2020) 225701.
[11] A. Yamamoto, K. Sugita, A.G. Bhuiyan, A. Hashimoto, N. Narita, Metal–organic vapor-phase epitaxial growth of InGaN and InAlN for multi-junction tandem solar cells, Mater. Renew. Sustain. Energy 2 (2) (2013) 1–9.
[12] C.A.M. Fabien, W.A. Doolittle, Guidelines and limitations for the design of high-efficiency InGaN single-junction solar cells, Sol. Energy Mater. Sol. Cells 130 (2014) 354–363.
[13] S. Ould Saad Hamady, A. Adaine, N. Fressengeas, Numerical simulation of InGaN Schottky solar cell, Mater. Sci. Semicond. Process. 41 (2016) 219–225.
[14] S. Sakai, Homoepitaxial and heteroepitaxial growth of InGaN/GaN, Electron. Commun. Japan 83 (2) (2000) 17–25.
[15] F.K. Yam, Z. Hassan, Ingan: An overview of the growth kinetics, physical properties and emission mechanisms, Superlattices Microstruct. 43 (1) (2008) 1–23.
[16] H. Ekinci, V.V. Kuryatkov, C. Forgey, A. Dabiran, R. Jorgenson, S.A. Nikishin, Properties of ingan/gan mqw leds grown by mocvd with and without hydrogen carrier gas, Vacuum 148 (2018) 168–172.
[17] B. Arnaudov, T. Paskova, S. Evtimova, E. Valcheva, M. Heuken, B. Monemar, Multilayer model for Hall effect data analysis of semiconductor structures with step-changed conductivity, Phys. Rev. B 67 (4) (2003) 045314.
[18] J. Olea, G. Gonzalez-Diaz, D. Pastor, I. Martil, A. Marti, E. Antolin, A. Luque, Two-layer hall effect model for intermediate band ti-implanted silicon, J. Appl. Phys. 109 (6) (2011) 063718.
[19] R.D. Larrabee, W.R. Thurber, Theory and application of a two-layer hall technique, IEEE Trans. Electron Devices 27 (1) (1980) 32–36.

[20] Yong. Huang, Growth and characterization of In(x)Ga(1-x)N alloys by metalorganic chemical vapor deposition for solar cell applications, J. Photon. Energy 2 (1) (2012) 028501.
[21] K. Prabakaran, R. Ramesh, P. Arivazhagan, M. Jayasakthi, S. Sanjay, S. Surender, S. Pradeep, M. Balaji, K. Baskar, Effects of indium flow rate on the structural, morphological, optical and electrical properties of InGaN layers grown by metal organic chemical vapour deposition, J Alloys and Compd. 811 (2019) 151803.
[22] P. Chan, S.P. DenBaars, S. Nakamura, Growth of highly relaxed InGaN pseudo-substrates over full 2-in. wafers, Appl. Phys. Lett. 119 (13) (2021) 131106.
[23] A.S. Yusof, Z. Hassan, S. Ould Saad Hamady, S.S. Ng, M.A. Ahmad, W.F. Lim, M.A.C. Seliman, C. Chevallier, N. Fressengeas, The role of growth temperature on the indium incorporation process for the MOCVD growth of InGaN/GaN heterostructures, Microelectron. Int. (2021).
[24] G. Liu, J. Zhang, X.H. Li, G.S. Huang, T. Paskova, K.R. Evans, H. Zhao, N. Tansu, Metalorganic vapor phase epitaxy and characterizations of nearly-lattice-matched AlInN alloys on GaN/sapphire templates and free-standing GaN substrates, J. Cryst. Growth 340 (1) (2012) 66–73.
[25] R. Butté, L. Lahourcade, T.K. Uždavinys, G. Callsen, M. Mensi, M. Glauser, G. Rossbach, D. Martin, J.F. Carlin, S. Marcinkevičius, et al., Optical absorption edge broadening in thick InGaN layers: Random alloy atomic disorder and growth mode induced fluctuations, Appl. Phys. Lett. 112 (3) (2018) 032106.
[26] W. Van der Stricht, I. Moerman, P. Demeester, L. Considine, E.J. Thrush, J.A. Crawley, Movpe growth optimization of high quality ingan films, Mater. Res. Soc. Internet J. Nitride Semicond. Res. 2 (1997).
[27] Z. Liu, S. Nitta, Y. Robin, M. Kushimoto, M. Deki, Y. Honda, M. Pristovsek, H. Amano, Morphological study of ingan on gan substrate by supersaturation, J. Cryst. Growth 508 (2019) 58–65.
[28] A. Tian, J. Liu, L. Zhang, L. Jiang, M. Ikeda, S. Zhang, D. Li, P. Wen, Y. Cheng, X. Fan, et al., Significant increase of quantum efficiency of green ingan quantum well by realizing step-flow growth, Appl. Phys. Lett. 111 (11) (2017) 112102.
[29] M.A. Laurent, S. Keller, U.K. Mishra, Comprehensive analysis of surface morphology and growth mode of alingan films, Phys. Status Solidi 216 (1) (2019) 1800523.
[30] D. Kim, K.M. Song, U.J. Jung, S. Kim, D.S. Shin, J. Park, Effects of different ingan/gan electron emission layers/interlayers on performance of a uv-a led, Appl. Sci. 10 (4) (2020) 1514.
[31] P. Pampili, P.J. Parbrook, Doping of III-nitride materials, Mater. Sci. Semicond. Process. 62 (2017) 180–191.
[32] J.L. Lyons, D. Wickramaratne, C.G. Van de Walle, A first-principles understanding of point defects and impurities in gan, J. Appl. Phys. 129 (11) (2021) 111101.
[33] M. Lozac'h, Y. Nakano, L. Sang, K. Sakoda, M. Sumiya, Study of defect levels in the band gap for a thick InGaN film, Japan. J. Appl. Phys. 51 (12R) (2012) 121001.
[34] T. Obata, J. Iwata, K. Shiraishi, A. Oshiyama, First principles studies on In-related nitride semiconductors, J. Cryst. Growth 311 (10) (2009) 2772–2775.
[35] B. Kucukgok, X. Wu, X. Wang, Z. Liu, I.T. Ferguson, N. Lu, The structural properties of InGaN alloys and the interdependence on the thermoelectric behavior, AIP Adv. 6 (2) (2016) 025305.